DOI: 10.1002/chem.201102603

Fluorescent Composite Hydrogels of Metal–Organic Frameworks and Functionalized Graphene Oxide

Ji Ha Lee,[a] Sunwoo Kang,[b] Justyn Jaworski,[a, c] Ki-Young Kwon,[a] Moo Lyong Seo,[a] Jin Yong Lee,*[b] and Jong Hwa Jung*[a]

Graphene and its functionalized derivatives are versatile building blocks for carbon-based materials, because of the unique 2D or 3D structures and excellent physical and chemical properties.[1–9] Recent work has demonstrated that self-assembly is a powerful technique for constructing hierarchical graphene-based nanomaterials with novel functions.[10–14] In particular, self-assembly of nanosized graphene into macroscopic materials can translate the properties of individual graphene sheets into the resulting macrostructures, which show numerous breakthrough applications in optoelectronics,[15] energy storage,[16–18] and biomedicine.[19–21] For example, transparent conducting membranes[22–24] and strong, layered, paperlike materials[25–27] have been prepared by various 2D self-assembly methods, including flow-directed self-assembly, layer-by-layer deposition, and Langmuir–Blodgett techniques.

Very recently, graphene-based metal–organic frameworks (MOFs) have been used by several groups to demonstrate 3D macroassemblies, due to the high porosity, the adsorption capacity for specific gases, and the electric properties of the MOFs.[28–31] For example, Loh and co-workers reported the synthesis of a crystalline MOF–graphene oxide composite.[28] Benzoic-acid-functionalized graphene acted as a structure-directing template that influenced the crystal growth of the MOF. The nanowire obtained from the benzoic-acid-functionalized graphene with MOF structure also imparted new electrical properties, such as photoelectric transport. However, the work on 3D self-assembly of graphene and its functionalized derivatives is still limited.[27–30] More facile and mild assembly strategies are needed for fabrication of multifunctional, 3D, graphene macrostructures. Alternatively, graphene-oxide-based hydrogels with MOF structures possess similar properties and are relatively rapid, efficient, and easy to prepare under mild conditions compared with crystalline MOFs. With this in mind, we report herein the formation of MOF–azobenzoic-acid-functionalized graphene-oxide hydrogels (MOF–A-GO) in the presence of Zn^{2+} and its application as a chemosensor for the detection of trinitrotoluene (TNT) molecules.

The preparation of azobenzoic acid (**2**)-functionalized graphene oxide (A-GO) is shown in Scheme 1. Initially, epoxy, and hydroxyl groups were removed by reduction with $NaBH_4$. Next, the chemically reduced GO (r-GO) was functionalized with azobenzoic acid (Scheme 1 and S1 in the Supporting Information) by using the diazonium grafting method, and this allowed the basal planes to become extended by azobenzoic-acid groups. A-GO was characterized by UV/Vis, FTIR, X-ray photoelectron spectroscopy (XPS), SEM, and TEM. Figure S1 in the Supporting Information shows the UV/Vis absorption spectra of GO, r-GO, and A-GO in water. The redshifted π–π^* absorption band of r-GO at 260 nm compared with the band of GO at 241 nm is consistent with the partial recovery of the conjugated network. In addition, absorption appeared at 400 nm, which is a typical wavelength for the azobenzoic acid attached to r-GO; this strongly indicates that the azobenzoic-acid moiety exists on the surface of r-GO. Moreover, A-GO shows improved dispersion in water compared with r-GO. The solution dispersability of A-GO was examined with UV/vis spectroscopy. A linear relationship between absorbance and concentration is observed in water; this is indicative of good dispersion of A-GO.

Figure S2 in the Supporting Information shows the FTIR spectra of r-GO and A-GO. The vibrational peaks of r-GO appeared at 1718, 1678, and 1060 cm^{-1} for C=O, C–OH, and C–O, respectively. On the other hand, new vibrational peaks of A-GO appeared at 3012, 1638, 1598, and 1430 cm^{-1} for aromatic C–H streches, C=O, and C=C ring stretches of the azobenzoic-acid groups, respectively. This is also indicative of attachment of the azobenzoic-acid moiety to the surface of r-GO by covalent bonding. r-GO was further confirmed by XPS before and after immobilization of azobenzoic acid (Figure S3 in the Supporting Information). The XPS spectrum of r-GO before immobilization of azobenzoic acid shows C1s and O1s binding energy (Figure S3a in the Sup-

[a] J. H. Lee, Prof. Dr. J. Jaworski, Prof. Dr. K.-Y. Kwon, Prof. Dr. M. L. Seo, Prof. Dr. J. H. Jung
Department of Chemistry and Research Institute of Natural Sciences, Gyeongsang National University
Jinju 660-701 (Korea)
Fax: (+82) 55-772-1488
E-mail: jonghwa@gnu.ac.kr

[b] S. Kang, Prof. Dr. J. Y. Lee
Department of Chemistry and Institute of Basic Science
Sungkyunkwan University, Suwon 440-746 (Korea)
E-mail: jinylee@skks.edu

[c] Prof. Dr. J. Jaworski
Department of Chemical Engineering
Hanyang University, Seoul 133-791 (Korea)

Supporting information for this article is available on the WWW under http://dx.doi.org/10.1002/chem.201102603.

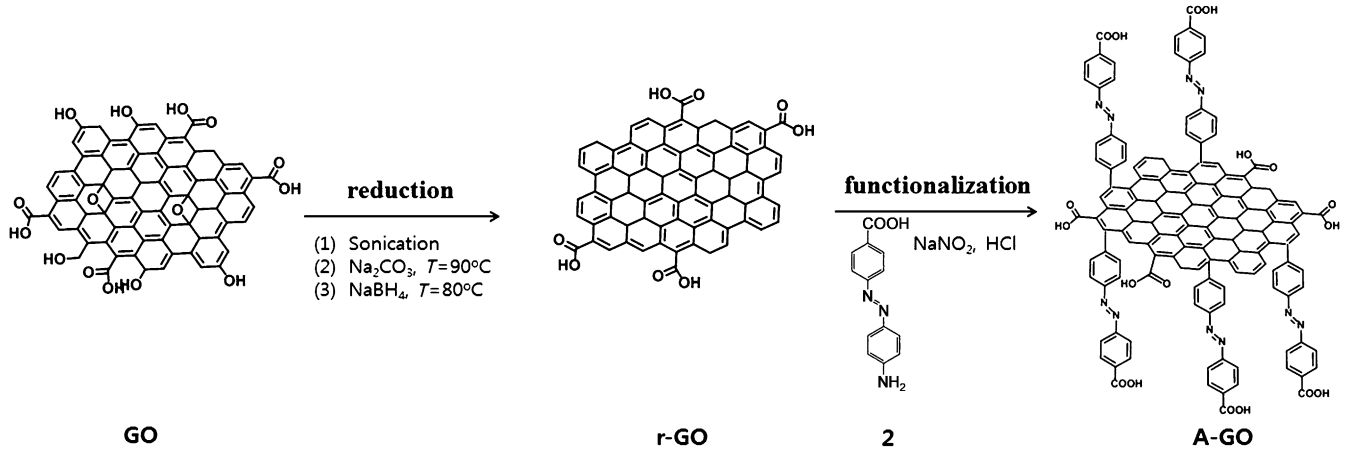

Scheme 1. Synthetic route of A-GO.

portign Information), whereas N1s for nitrogen appeared in A-GO (Figure S3b).

A-GO was further confirmed by TEM and electron energy loss spectroscopy (EELS, Figure 1). The material contained carbon, oxygen, and nitrogen components, supporting the idea that azobenzoic acid is homogenously attached to the surface of r-GO. Figure 1B shows the atomic force microscopy (AFM) image of an A-GO sheet, and Figure 1C shows the corresponding height profile. It shows that the A-GO monolayer is regular with a height of 1.0 nm, indicating that A-GO consists of a monolayer sheet.

When the A-GO (10 mg mL^{-1}) suspension with Zn^{2+} and ligand **1** (Scheme S2 in the Supporting Information) was

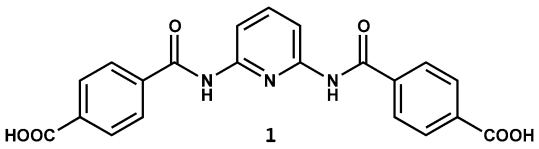

mixed by ultrasonication for a few seconds, the MOF–A-GO composite hydrogel was obtained as shown in Figure 2A. On the other hand, ligand **1** with Zn^{2+} did not form the hydrogel at the same concentration. These findings sug-

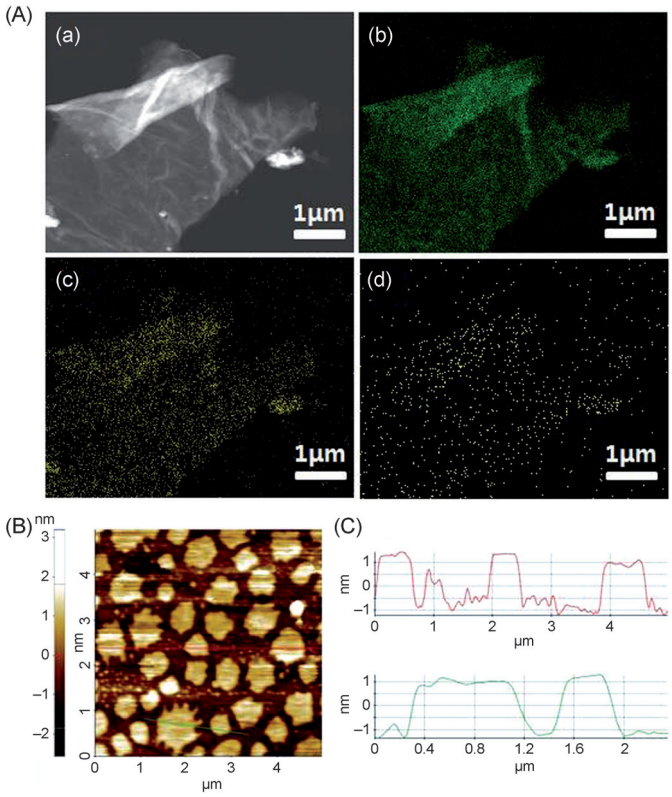

Figure 1. A) EELS-TEM images of A-GO; a) zero-loss image, b) carbon, c) oxygen, and d) nitrogen components. B) AFM image of A-GO and C) the height profile.

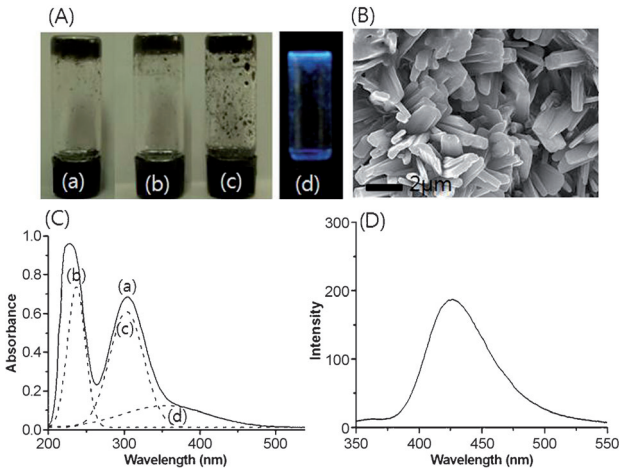

Figure 2. A) Photograph of MOF-A-GO composites hydrogels; a) 1:1:1 (metal/ligand/GO), b) 1:1:2, c) 1:1:3 mole ratios, d) sample in (c) irradiated with UV lamp. B) SEM image of a MOF-A-GO composites hydrogel formed by a 1:1:3 (metal/ligand/GO) mole ratio. C) UV/Vis spectra of a) the MOF–A-GO composite hydrogel (1:1:3 mole ratio), b) r-GO, c) A-GO, and d) ligand **1** obtained from (a) with curve fitting. D) Fluorescence spectrum of the MOF–A-GO composite hydrogel (1:1:3 mole ratio).

gest that A-GO acted as an interlayer to form the stable MOF structure in the gel phase.

To gain insight into the morphology of the MOF–A-GO composite hydrogel induced by both A-GO and ligand **1** in the presence of Zn^{2+}, we observed a xerogel of MOF–A-GO by SEM (Figure 2B). The morphology of MOF–A-GO is quite different from that of A-GO. MOF–A-GO has a well-defined nanorod structure with a width of 100–150 nm and a length of several micrometers. The sheet structure of A-GO was not obtained in MOF–A-GO. The results support the view that A-GO is bound to ligand **1** by a coordination bond with Zn^{2+}; this forms the MOF structure.

The absorption and emission properties of A-GO, sol **1**, and MOF–A-GO in the presence of Zn^{2+} were extensively studied. The UV/Vis absorption band of MOF–A-GO with Zn^{2+} appears at 302 nm and 367 nm, respectively (Figure 2C), typical of a π–π^* transition for the self-assembled ligand **1** and the azobenzoic-acid moiety.[32,33] The fluorescence spectrum of MOF–A-GO ($\lambda_{ex}=302$ nm) was also obtained (Figure 2D). Interestingly, MOF–A-GO exhibits a strong blue emission with a maximum at $\lambda=425$ nm. The fluorescence intensity is enhanced drastically compared with sol **1**. The photoluminescence of MOF–A-GO can be seen by the naked eye under UV light (Figure 2A d). The fluorescence intensity of MOF–A-GO gradually increased with the addition of metal ion until 1.0 equivalent had been added and then remained constant upon further additions (Figure S4 in the Supporting Information). These results indicate that one molecule of ligand **1** binds to one Zn^{2+} ion. The luminescence properties of MOF–A-GO were studied by time-resolved fluorescence confocal microscopy. The emission-decay profiles were monitored at $\lambda=405$–490 nm for MOF–A-GO. The fluorescence decay of MOF–A-GO was fitted with a single exponential component, yielding a lifetime of 2.75 ns (Figure S5 in the Supporting Information), which indicates that this emission is fluorescence. This result reflects the fact that MOF–A-GO in the aggregate state is more rigid and restricts the rotational and vibrational movements of the molecules. The limited molecular motions decrease the nonradiative relaxation process; this leads to a longer lifetime and fluorescence enhancement.[34] In contrast, the lifetime of sol **1** is much shorter than that of MOF–A-GO.

Zn^{2+} is known to have T_d- or O_h-coordinated structures with certain ligands.[35,36] To understand the nature of the coordination conformation of Zn^{2+}, the favored coordinated structure needs to be considered. Hence, we have carried out density functional theory (DFT) calculations for T_d and O_h structures by employing the hybrid functional of Becke's three parameterized Lee–Yang–Parr with the 6-31G* basis sets and a suite of Gaussian 09 programs.[37] From the optimized structures, we concluded that the T_d structure should be the major product, as is shown in Figure 3. The interatomic distances between the oxygen atoms of the ligands (**1** and A-GO) and Zn^{2+} were calculated to be 1.937–1.976 Å. The substituted azobenzoic moieties break the planarity of GO.

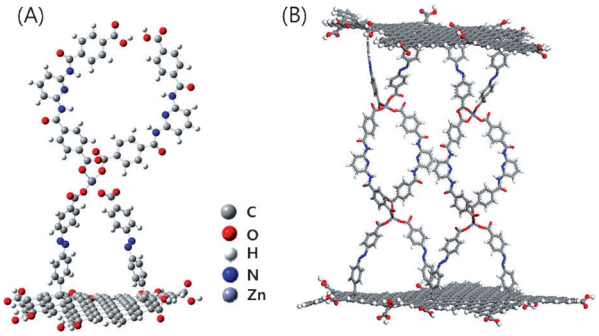

Figure 3. A) Representation of proposed bonding between **1** and A-GO in the presence of Zn^{2+}. B) The expanded A-GO with two Zn^{2+} and four **1** optimized by MM calculation. (The GO sheet is denoted as balls and sticks. The rest of moieties are denoted as sticks.)

By using the structural parameters and geometrical features of the optimized structure, the expanded size of A-GO with two Zn^{2+} and four **1** was generated (Figure 3B). This expanded structure was simply optimized with MM calculations by employing a universal force field due to computational capabilities. The interatomic distance between the two Zn^{2+} atoms was calculated to be 18.37 Å and that between pyridine nitrogens of two molecules of ligand **1** was calculated to be 8.82 Å, which indicates that a sufficient cavity size exsists. Consequently, it would be expected from the structural feature that the cavity can act as a recognition site for certain guest molecules through hydrogen binding or π–π^* stacking.

Fluorescence of MOF–A-GO was also measured as a function of temperature (Figure S6 in the Supporting Information). No significant spectral changes were observed below 100 °C. The fluorescence intensity of MOF–A-GO slightly decreases at 105 °C. Further increases in temperature resulted in a large decrease in emission. These results suggest that the emission of MOF–A-GO decreases as it starts to melt at 105–110 °C. The optimal emission of MOF–A-GO therefore occurs when the gel is completely formed and decreases as the gel melts at higher temperature. This striking observation may be attributed to the rigidification of the media upon gelation, a process that slows down nonradiative-decay mechanisms and leads to luminescence enhancement. Even though the gel dissociates from the aggregated state and shows a drastic drop in fluorescence intensity, the complex still exhibits a considerable blue emission in the solution state. This may be due to weak supramolecular interactions while still in the solution state.

To gain insight into the thermally promoted stability of MOF–A-GO, the sol–gel transition temperature (T_{gel}) of MOF–A-GO was measured by differential scanning calorimetry (DSC, Figure S7 in the Supporting Information). The MOF–A-GO composite gel showed a sharp phase transition at 107 °C; this indicated an endothermic reaction. This endothermic thermogram was attributed to the change of MOF–A-GO into a sol state (Figure S8 in the Supporting Information). This T_{gel} of MOF–A-GO is consistent with the results obtained by fluorescence spectroscopy.

Rheological information aids in understanding the behavior of gels when they are exposed to mechanical stress, especially the "storage" (or "elastic") modulus G′, which represents the ability of the deformed material to "snap back" to the original geometry, and the "loss" (or "viscous") modulus G″, which represents the tendency of a material to flow under stress. Two rheological criteria are required for a gel: 1) the dynamic G′ has to be independent of the oscillatory frequency, and 2) G′ should exceed G″ by about one order of magnitude. We first used a dynamic strain sweep to determine the proper condition for the subsequent examination of the gel under a dynamic frequency sweep. As shown in Figure S8A in the Supporting Information, the values of G′ and G″ exhibited a weak strain dependence from 0.1 to 1.0% (with G′ dominating G″); this indicates that the sample is a gel. After setting the strain amplitude to 0.8% (within the linear response regime for strain amplitute), we used a dynamic frequency sweep to further study the gel. Figure S8B demonstrates that G′ and G″ are almost constant despite an increase in frequency from 0.1 to 100 rad s^{-1}. The value of G′ is about five times larger than that of G″ over the whole range (0.1–100 rad s^{-1}), suggesting that the gel is fairly tolerant to external forces. Furthermore, time-dependent oscillation measurements were used to monitor the gelation process of MOF–A-GO, which forms gradually upon mixing of A-GO and ligand **1** in the presence of Zn^{2+} (Figure S8C). The time-sweep results show the rapid growth of G′ and G″ in the initial stage of gelation followed by a slower long-term approach to a final pseudo-equilibrium plateau. At the end of the experiment, the value of G′ was about an order-of-magnitude higher than G″.

To investigate the applicability of MOF–A-GO as a portable chemosensor kit, the sensing ability was studied in the film state by exposing films to trinitrotoluene (TNT) and dinitrotoluene (DNT) vapors (Figure 4). Films of MOF–A-GO were drop casted from water, and the films showed 70% fluorescence quenching after one minute of exposure to saturated TNT vapors. Nearly 98% quenching was observed upon continuous exposure for 10 min (Figure 4b). As expected, the MOF–A-GO film exhibited a gradual decrease in fluorescent intensity upon the addition of TNT; this is attributed to charge-transfer interactions between the electron-deficient aromatic ring of TNT and the electron-rich aromatic group of **1** in MOF–A-GO. The use of MOF–A-GO for the detection of DNT vapors was also studied. A film of MOF–A-GO showed a quenching effect on fluorescence when exposed to saturated DNT vapors under the same conditions; however, the quenching efficiency was found to be much less than that of TNT vapors. After exposure for 10 min, only 2% quenching was observed in the presence of DNT compared with 98% quenching for TNT.

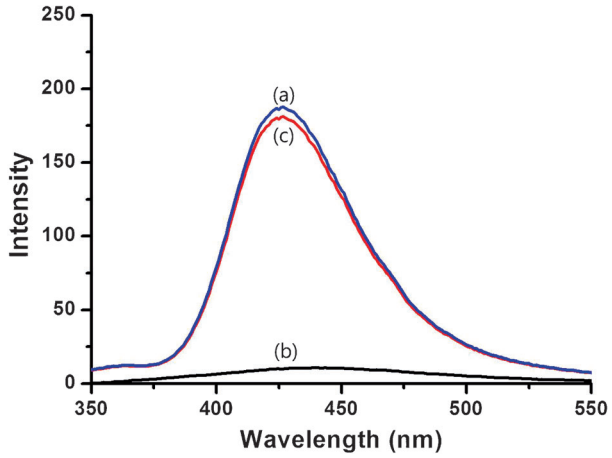

Figure 4. Fluorescence spectra of a MOF–A-GO composite hydrogel film a) before and after immersion of b) TNT (1.0 μmol) and c) DNT (1.0 μmol).

We also carried out DFT calculations for the charge-transfer interaction between the TNT molecules and **1** in MOF–A-GO by using Becke's three parameterized Lee–Yang–Parr with the 6-31G* basis sets and a suite of Gaussian 09 programs.[37] According to preliminary computational simulations, TNT molecules can be inserted into the cavity of the Zn^{2+} complex, and binds tightly through the charge-transfer interaction inside the cavity (Figure S9 in the Supporting Information). In addition, the charge-transfer interaction between the TNT molecules and **1** in the MOF–A-GO composite hydrogel was much stronger than that of DNT.

In conclusion, we have demonstrated that the formation the MOF–A-GO composite hydrogel can be achieved. The A-GO is shown to efficiently produce a hydrogel by simple mixing with **1** in the presence of Zn^{2+}. This is the first example of a graphene-based MOF–GO composite hydrogel. Photophysical studies show that the hydrogel exhibits a typical π–π* transition and gives rise to highly fluorescent behavior. Upon the formation of the MOF–A-GO composite hydrogel, the complex shows a pronounced fluorescence enhancement with a long lifetime, compared with that of the ligand. Together, measurements of dynamic oscillation and steady shear indicate the formation of a weak and thermally labile network for which the tenuous supramolecular structure is irreversibly disrupted by mechanical and thermal treatments. In addition, MOF–A-GO composite hydrogels can act as chemosensors, for example, for TNT detection. Graphene-based MOF hydrogels provide a powerful strategy for developing new molecularly defined materials in the areas of biology, medicine, and material science. We believe this could possibly provide a model system for sensors, catalysis, and delivery.

Acknowledgements

This work was supported by a grant from the World Class University (WCU) Program (R32-2008-000-20003-0) and the NRF (2011-0005689) supported from the Ministry of Education, Science, and Technology, S. Korea.

Keywords: graphene oxide · gels · metal–organic frameworks · trinitrotoluene

[1] A. K. Geim, *Science* **2009**, *324*, 1530–1534.
[2] C. N. R. Rao, A. K. Sood, K. S. Subrahmanyam, A. Govindaraj, *Angew. Chem.* **2009**, *121*, 7890–7916; *Angew. Chem. Int. Ed.* **2009**, *48*, 7752–7777.
[3] O. C. Compton, S. T. Nguyen, *Small* **2010**, *6*, 711–723.
[4] C. Huang, H. Bai, C. Li, G. Shi, *Chem. Commun.* **2011**, *47*, 4962–4964.
[5] J. Shen, Y. Zhu, C. Chen, X. Yang, C. Li, *Chem. Commun.* **2011**, *47*, 2580–2582.
[6] J. Balapanuru, J.-X. Yang, S. Xiao, Q. Bao, M. Jahan, L. Polavarapu, J. Wei, Q.-H. Xu, K. P. Loh, *Angew. Chem.* **2010**, *122*, 6699–6703; *Angew. Chem. Int. Ed.* **2010**, *49*, 6549–6553.
[7] Q. Ji, I. Honma, S.-M. Paek, M. Akada, J. P. Hill, A. Vinu, K. Ariga, *Angew. Chem.* **2010**, *122*, 9931–9933; *Angew. Chem. Int. Ed.* **2010**, *49*, 9737–9739.
[8] V. Dua, S. P. Surwade, S. Ammu, S. R. Agnihotra, S. Jain, K. E. Roberts, S. Park, R. S. Ruoff, S. K. Manohar, *Angew. Chem.* **2010**, *122*, 2200–2203; *Angew. Chem. Int. Ed.* **2010**, *49*, 2154–2157.
[9] H. Li, S. Pang, S. Wu, X. Feng, K. Müllen, C. Bubeck, *J. Am. Chem. Soc.* **2011**, *133*, 9423–9429.
[10] D. Li, R. B. Kaner, *Science* **2008**, *320*, 1170–1171.
[11] Y. X. Xu, L. Zhao, H. Bai, W. J. Hong, C. Li, G. Q. Shi, *J. Am. Chem. Soc.* **2009**, *131*, 13490–13497.
[12] C. X. Guo, H. B. Yang, Z. M. Sheng, Z. S. Lu, Q. L. Song, C. M. Li, *Angew. Chem.* **2010**, *122*, 3078–3081; *Angew. Chem. Int. Ed.* **2010**, *49*, 3014–3017.
[13] S. Yang, X. Feng, L. Wang, K. Tang, J. Maier, K. Mullen, *Angew. Chem.* **2010**, *122*, 4905–4909; *Angew. Chem. Int. Ed.* **2010**, *49*, 4795–4799.
[14] H. Bai, C. Li, X. L. Wang, G. Q. Shi, *Chem. Commun.* **2010**, *46*, 2376–2378.
[15] G. Eda, M. Chhowalla, *Adv. Mater.* **2010**, *22*, 2392–2415.
[16] D. W. Wang, F. Li, J. P. Zhao, W. C. Ren, Z. G. Chen, J. Tan, Z. S. Wu, I. Gentle, G. Q. Lu, H. M. Cheng, *ACS Nano* **2009**, *3*, 1745–1752.
[17] D. H. Wang, R. Kou, D. Choi, Z. G. Yang, Z. M. Nie, J. Li, L. V. Saraf, D. H. Hu, J. G. Zhang, G. L. Graff, J. Liu, M. A. Pope, I. A. Aksay, *ACS Nano* **2010**, *4*, 1587–1595.
[18] J. K. Lee, K. B. Smith, C. M. Hayner, H. H. Kung, *Chem. Commun.* **2010**, *46*, 2025–2027.
[19] H. Chen, M. B. Muller, K. J. Gilmore, G. G. Wallace, D. Li, *Adv. Mater.* **2008**, *20*, 3557–3561.
[20] A. J. Patil, J. L. Vickery, T. B. Scott, S. Mann, *Adv. Mater.* **2009**, *21*, 3159–3164.
[21] S. Park, N. Mohanty, J. W. Suk, A. Nagaraja, J. H. An, R. D. Piner, W. W. Cai, D. R. Dreyer, V. Berry, R. S. Ruoff, *Adv. Mater.* **2010**, *22*, 1736–1740.
[22] G. Eda, G. Fanchini, M. Chhowalla, *Nat. Nanotechnol.* **2008**, *3*, 270–274.
[23] X. L. Li, G. Y. Zhang, X. D. Bai, X. M. Sun, X. R. Wang, E. Wang, H. J. Dai, *Nat. Nanotechnol.* **2008**, *3*, 538–542.
[24] L. J. Cote, F. Kim, J. X. Huang, *J. Am. Chem. Soc.* **2009**, *131*, 1043–1049.
[25] D. A. Dikin, S. Stankovich, E. J. Zimney, R. D. Piner, G. H. B. Dommett, G. Evmenenko, S. T. Nguyen, R. S. Ruoff, *Nature* **2007**, *448*, 457–460.
[26] D. Li, M. B. Muller, S. Gilje, R. B. Kaner, G. G. Wallace, *Nat. Nanotechnol.* **2008**, *3*, 101–105.
[27] Y. X. Xu, H. Bai, G. W. Lu, C. Li, G. Q. Shi, *J. Am. Chem. Soc.* **2008**, *130*, 5856–5857.
[28] M. Jahan, Q. Bao, J.-X. Yang, K. P. Loh, *J. Am. Chem. Soc.* **2010**, *132*, 14487–14495.
[29] C. Petit, T. J. Bandosz, *Adv. Funct. Mater.* **2010**, *20*, 111–118.
[30] J. W. Burress, S. Gadipelli, J. Ford, J. M. Simmons, W. Zhou, T. Yildirim, *Angew. Chem.* **2010**, *122*, 9086–9088; *Angew. Chem. Int. Ed.* **2010**, *49*, 8902–8904.
[31] C. Petit, T. J. Bandosz, *Adv. Mater.* **2009**, *21*, 4753–4757.
[32] L. A. Estroff, A. D. Hamilton, *Chem. Rev.* **2004**, *104*, 1201–1218.
[33] N. M. Sangeetha, U. Maitra, *Chem. Soc. Rev.* **2005**, *34*, 821–836.
[34] J. H. Lee, H. Lee, S. Seo, M. L. Seo, S. Kang, J. Y. Lee, J. H. Jung, *New J. Chem.* **2011**, *35*, 1054–1057.
[35] C. A. Bauer, T. V. Timofeeva, T. B. Settersten, B. D. Patterson, V. H. Liu, B. A. Simmons, M. D. Allendorf, *J. Am. Chem. Soc.* **2007**, *129*, 7136–7144.
[36] M. Dincă, A. F. Yu, J. R. Long, *J. Am. Chem. Soc.* **2006**, *128*, 8904–8913.
[37] Gaussian 03, Revision B05, M. J. Frisch, G. W. Trucks, H. B. Schlegel, G. E. Scuseria, M. A. Robb, J. R. Cheeseman, J. A. Montgomery, Jr., T. Vreven, K. N. Kudin, J. C. Burant, J. M. Millam, S. S. Iyengar, J. Tomasi, V. Barone, B. Mennucci, M. Cossi, G. Scalmani, N. Rega, G. A. Petersson, H. Nakatsuji, M. Hada, M. Ehara, K. Toyota, R. Fukuda, J. Hasegawa, M. Ishida, T. Nakajima, Y. Honda, O. Kitao, H. Nakai, M. Klene, X. Li, J. E. Knox, H. P. Hratchian, J. B. Cross, V. Bakken, C. Adamo, J. Jaramillo, R. Gomperts, R. E. Stratmann, O. Yazyev, A. J. Austin, R. Cammi, C. Pomelli, J. W. Ochterski, P. Y. Ayala, K. Morokuma, G. A. Voth, P. Salvador, J. J. Dannenberg, V. G. Zakrzewski, S. Dapprich, A. D. Daniels, M. C. Strain, O. Farkas, D. K. Malick, A. D. Rabuck, K. Raghavachari, J. B. Foresman, J. V. Ortiz, Q. Cui, A. G. Baboul, S. Clifford, J. Cioslowski, B. B. Stefanov, G. Liu, A. Liashenko, P. Piskorz, I. Komaromi, R. L. Martin, D. J. Fox, T. Keith, M. A. Al-Laham, C. Y. Peng, A. Nanayakkara, M. Challacombe, P. M. W. Gill, B. Johnson, W. Chen, M. W. Wong, C. Gonzalez, J. A. Pople, Gaussian, Inc., Wallingford CT, **2004**.

Received: August 22, 2011
Published online: December 13, 2011

